



## OPEN ACCESS

## EDITED BY

Tavishi Tewary,  
Fore School of Management, India

## REVIEWED BY

Deep Raj,  
SRM University, India  
Aneek Kuila,  
Technion Israel Institute of Technology, Israel

## \*CORRESPONDENCE

Nitin Pratap Varma,  
✉ nitinpratapvarma@yahoo.com  
Jaydev Kumar Mahato,  
✉ jay\_devkumar@rediff.com

RECEIVED 05 January 2024

ACCEPTED 07 February 2024

PUBLISHED 05 March 2024

## CITATION

Varma NP, Sinha A, Gupta SK, Mahato JK and Chand P (2024), Enhanced defluoridation by nano-crystalline alum-doped hydroxyapatite and artificial intelligence (AI) modeling approach.

*Front. Environ. Sci.* 12:1363724.

doi: 10.3389/fenvs.2024.1363724

## COPYRIGHT

© 2024 Varma, Sinha, Gupta, Mahato and Chand. This is an open-access article distributed under the terms of the [Creative Commons Attribution License \(CC BY\)](#). The use, distribution or reproduction in other forums is permitted, provided the original author(s) and the copyright owner(s) are credited and that the original publication in this journal is cited, in accordance with accepted academic practice. No use, distribution or reproduction is permitted which does not comply with these terms.

# Enhanced defluoridation by nano-crystalline alum-doped hydroxyapatite and artificial intelligence (AI) modeling approach

Nitin Pratap Varma<sup>1\*</sup>, Alok Sinha<sup>1</sup>, Sunil Kumar Gupta<sup>1</sup>, Jaydev Kumar Mahato<sup>1\*</sup> and Priyankar Chand<sup>2</sup>

<sup>1</sup>Department of Environmental Science and Engineering, Indian Institute of Technology, Dhanbad, India,

<sup>2</sup>Environmental Science and Engineering Department, Indian Institute of Technology Bombay, Mumbai, India

The study aimed to investigate the defluoridation capacity of nano-hydroxyapatite (HAP) [Ca<sub>10</sub>(PO<sub>4</sub>)<sub>6</sub>(OH)<sub>2</sub>] and alum-doped hydroxyapatite (AHAP) [Ca<sub>8</sub>Al(PO<sub>4</sub>)<sub>6</sub>(OH)<sub>2</sub>] as an environmental friendly adsorbent. The physicochemical characteristics of both the material (HAP and AHAP) were examined using XRD, FE-SEM-EDS, and BET techniques. The batch adsorption study revealed a fluoride removal efficiency of up to 83% (AHAP) and 74% (HAP) under acidic conditions (pH=2). The doping of alum alters the surface chemistry and enhances the affinity of AHAP for fluoride adsorption. The pseudo-second-order kinetic (R<sup>2</sup>=0.9941) and Langmuir isotherm (R<sup>2</sup>=0.9425) models best describe the adsorption mechanism and behavior. The thermodynamic analysis indicated the spontaneous and endothermic nature of the adsorption process. The study also tested the applicability of the artificial neural network (ANN) modeling approach using MATLAB R2013a to simulate the simulated absorptive efficiency of AHAP. This study suggests that AHAP proved an effective adsorbent for defluoridation.

## KEYWORDS

nano-hydroxyapatite, alum, defluoridation, Bangham kinetics, ANN

## 1 Introduction

Fluoride is one of the most profuse elements and is found in groundwater around the globe. For both humans and animals, it is a crucial trace element (Shaji et al., 2024). The potential benefits or hazards of fluoride in water are determined by its concentration and the overall quantity consumed. The impact of fluoride levels in drinking water extends beyond human health, affecting various living organisms. Elevated fluoride concentrations influence the tissues of osseous (teeth and bones) and soft (liver, kidney, brain, etc.) (Jagtap et al., 2012; Ali et al., 2021; Choubisa et al., 2023). Additionally, alterations in the function and metabolism of the liver and kidneys are induced by increased fluoride levels (Yang et al., 2019; Singh et al., 2022). The main cause of fluoride in drinking water is the dissolution of fluoride-bearing minerals and rocks like fluorospar, cryolite, fluorite, and fluorapatite. However, unregulated industrial discharge is one of the biggest concerns pertaining to fluoride contamination (Chouhan and Flora, 2010). According to the World

Health Organization (WHO), 1.5 mg/L for drinking water and 8 mg/L for industrial discharge are the recommended maximum concentration limits (MCLs) (WHO, 2008). In groundwater, the amount of fluoride ions can reach more than 30 mg/L. The daily consumption of 20–80 mg of fluoride over the duration of 10–20 years causes skeletal fluorosis, which causes severe bone damage (Singh et al., 2016; Lacson et al., 2021). It has also been reported to cause dental fluorosis, DNA aberrations, neurological damage, and interference with normal organ metabolism (Xiong et al., 2007; WHO, 2008; Chen et al., 2011; Singh et al., 2016; Amalraj and Pius, 2017). Around 200 million people worldwide have been reported to be affected by fluoride pollution. Fluorosis has adversely impacted India, with more than 66 million individuals, including 6 million children under the age of 14, being affected by this prevalent geochemical disease (Ayoob and Gupta, 2006; Prasad et al., 2014). Thus, it is crucial to defluoridate drinking water that contains a high amount of fluoride to protect public health. As a result, different methods for defluoridating aqueous solutions have been developed over the past decade.

Defluoridation of potable water is achieved through various physical and chemical methods (Chouhan and Flora, 2010). Bio-sorbents made from plant materials and bacterial bioremediation are two biological methods for phytoremediation and defluoridation of the air. Defluoridation technologies have been described, viz., adsorption, chemical precipitation, electrocoagulation, nanofiltration, reverse osmosis, and ion exchange (Ahmad et al., 2015; Nkansah et al., 2022). Among them, adsorption, especially mineral-based and surface-modified adsorbents, has shown promising results in removing excess fluoride from water, and it is one popular method for defluoridation (Mohapatra et al., 2009; Bhatnagar et al., 2011; Loganathan et al., 2013). Hydroxyapatite,  $\text{Ca}_{10}(\text{PO}_4)_6(\text{OH})_2$  (HAP) as calcium phosphate-based bioceramics is widely used in biotechnology and medical applications to repair damaged parts of the body as an implant. HAP as an adsorbent has demonstrated comparatively good defluoridation performance in several studies (Bhatnagar et al., 2011; Tang et al., 2022). Previous studies have demonstrated that the HAP's surface hydroxyl groups are an active site for adsorption.

In current scenarios, significant efforts have been made to advance new and cost-effective sorbents for fluoride removal by impregnating low-cost adsorbents with chemicals, aiming to enhance defluoridation efficiency. Fluorine is a very undesirable element with a strange tendency to induce attraction by charged ions like metallic elements. Aluminum is frequently used in defluoridation methods due to its highly electropositive nature, which makes it easily able to interact with fluorine atoms. Tripathy et al. (2006) demonstrated 99% defluoridation performance using alum-impregnated activated alumina (Tripathy et al., 2006). Amalraj and Pius (2017) also demonstrated a significant fluoride adsorption efficiency of 26.03 mg/g using aluminum hydroxide-modified activated carbon. Hydroxyapatite has also been successfully modified with Aluminum (AHAP) to acquire an advanced defluoridation capacity of 32.57 mg F<sup>-</sup>/g than unmodified hydroxyapatite (HAP) with 16.38 mg F<sup>-</sup>/g capacity (Nie et al., 2012). Sasaki et al. (2017) have revealed that accelerated defluoridation results from the  $\text{Al}^{3+}$  ions' effective transport of F<sup>-</sup> to the hydroxyapatite/fluorapatite precursor.

Artificial Neural Network (ANN) has gained increasing consideration for water quality prediction and treatment modeling simulation in recent years. This approach is particularly suitable in applications where the mechanisms underlying process performance are highly complex and non-linear, such as the adsorption process. Hence, ANN is a suitable approach for modeling the adsorptive efficiency of adsorbents (Mahato and Gupta, 2022).

In this study, the influence of alum ( $\text{KAl}(\text{SO}_4)_2 \cdot 12\text{H}_2\text{O}$ ) on the adsorption of F<sup>-</sup> under biomimetically synthesized nano-crystalline HAP and Alum-doped HAP (AHAP) is examined. The adsorption parameter is studied beneath by contact time, pH, and reaction temperature on F<sup>-</sup> adsorption. Isotherms and kinetic models are also used to validate the experimental data. The kinetic, thermodynamic, and equilibrium analyses support the AHAP's adsorption mechanism. In addition, the adsorptive efficiency of AHAP was also simulated with the Artificial Neural Network (ANN) modeling approach using MATLAB R2013a.

## 2 Materials and methods

### 2.1 Chemicals

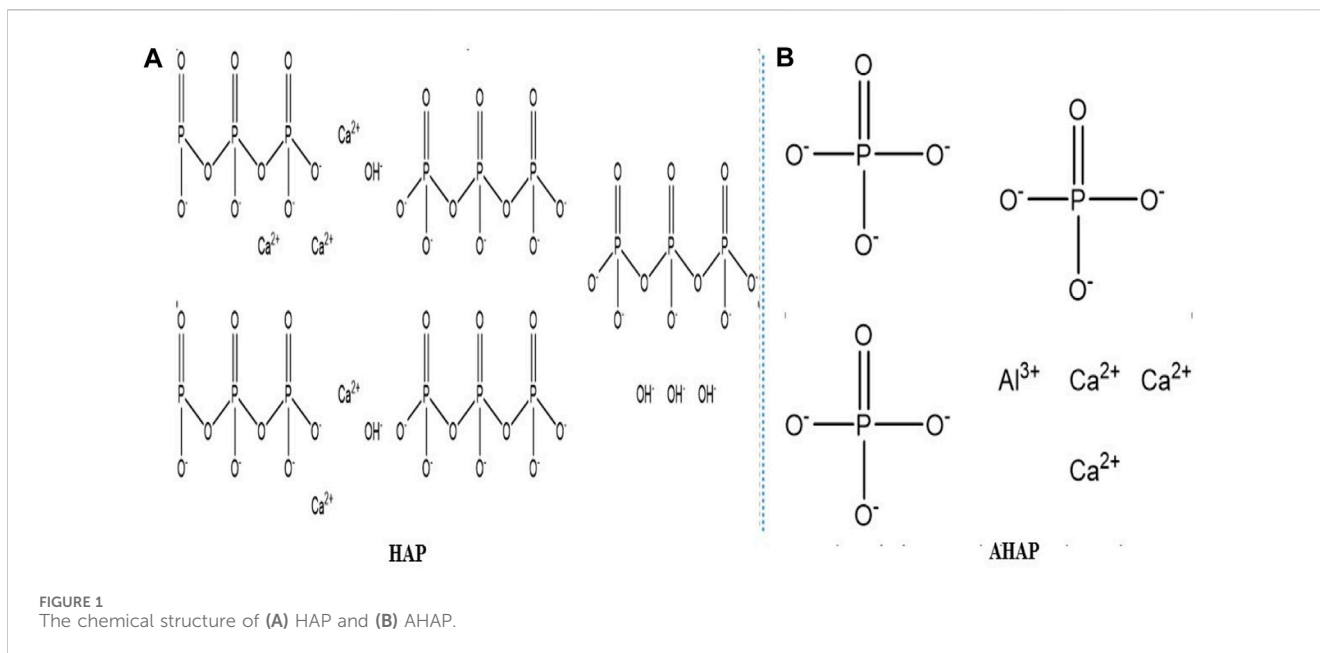
All the reagents used for synthesis include di-ammonium hydrogen phosphate [ $(\text{NH}_4)_2\text{HPO}_4$ ] (Merck, India) and calcium nitrate tetrahydrate [ $\text{Ca}(\text{NO}_3)_2 \cdot 4\text{H}_2\text{O}$ ] (Rankem, India). Ammonium solution and polyvinyl alcohol (PVA) were acquired from Acros Organics and used without supplementary refinement.

Analytical grade alum (Aluminium potassium sulfate dodecahydrate,  $\text{KAl}(\text{SO}_4)_2 \cdot 12\text{H}_2\text{O}$ ), sodium fluoride (NaF), sodium hydroxide (NaOH), and nitric acid ( $\text{HNO}_3$ ) were purchased from Merck (India). The stock solution of fluoride was prepared with deionized water using NaF, where  $\text{HNO}_3$  (0.1 M) and NaOH (0.1 M) solutions were used to adjust the pH of the solution.

### 2.2 Synthesis of Al-doped hydroxyapatite

Nano-hydroxyapatite (HAP) ( $\text{Ca}_{10}(\text{PO}_4)_6(\text{OH})_2$ ) was synthesized biomimetically using a chemical co-precipitation technique utilizing di-ammonium hydrogen phosphate and calcium nitrate tetrahydrate as precursors with PVA as stabilizing matrix, which controls the shape and size of HAP. The co-precipitation process is the most commonly used method for synthesizing HAP and has been discussed elsewhere (Sinha et al., 2003; Sinha et al., 2008). Setting the atomic ratio of [Ca + P] to 1.67 allowed the biomimetic synthesis of nano-hydroxyapatite (HAP).

Hydroxyapatite suspension was prepared using 5 g of dried HAP nanoparticles suspended in 100 mL double distilled water (DDW) followed by pH measurement of suspension (pH 7.5). To the suspension, 5.7 g of alum was added, and the pH was adjusted using 1N  $\text{HNO}_3$ . The suspension's final pH was set at 3, and it was stirred for 1.5 h at 70°C, followed by incubation for 1 h. Alum-doped HAP (AHAP) nanoparticles were obtained by processing the precipitates, cleaning them with DDW several times, and then air-drying them at 650°C for 24 h. The chemical structure of HAP and AHAP is illustrated in Figures 1A, B.



## 2.3 Characterization of the adsorbents

The superficial morphology of HAP and AHAP was characterized by a Scanning Electron Microscope (FE-SEM, Zeiss Supra 55VP, United States) on a high-resolution instrument equipped with a Gemini Field Emission Column and an Energy Dispersive X-ray Spectrometer (EDS) probe (Phoenix) equipped with a sapphire detector for digital signal processing for semi-quantitative chemical analysis. X-ray diffraction (XRD) patterns of synthetic HAP and AHAP were captured before and after fluoride adsorption on an X-ray powder diffractometer, the (XRD, Bruker Advanced X-Ray Solutions, GMBH, Germany) to examine the structure of the adsorbent. The specific surface area of the HAP and AHAP was determined by the BET surface area analyzer (NOVA 4000e, Quantachrome Instruments, United States).

## 2.4 Adsorption experiments

Batch adsorption experiments were carried out in 100 mL Erlenmeyer flasks using the working volume of 50 mL. The flasks were closed and kept in an orbital thermostat shaker (Rivotek, Kolkata, India) after adding HAP/AHAP (0.5 g/L) to the fluoride solution at 180 rpm for 1 h. The effect of pH was examined with different pH values, i.e., 2, 3, 4, 5, 6, 7, 8, and 9 on adsorption. The effect of contact time was also analyzed by shaking the sample for 6 h at optimum pH. The adsorption kinetics were carried out at a constant temperature of 303 K. The thermodynamic study was conducted at 293 K, 303 K, and 313 K. The fluoride concentration was measured using pH/ISE meter (Orion Model, EA 940 Expandable Ion Analyzer) attached to fluoride-selective electrode (Orion Model 96-09). The blank solution was also run parallelly for fluoride measurement. All the experiments were performed in triplicate.

The equilibrium uptake of fluoride was calculated using Eq. 1:

$$q_t = \frac{(C_0 - C_t)}{M} \cdot V \quad (1)$$

where  $q_t$  is the measure of fluoride adsorbed on the adsorbent (mg/g) at time  $t$ ,  $C_0$  is the initial concentration of  $F^-$  in solution ( $\text{mM}^{-1}$ ),  $C_t$  is the concentration of  $F^-$  in solution ( $\text{mg L}^{-1}$ ) after time  $t$ ,  $V$  is the volume of solution in (L) and  $W$  is the adsorbent weight (g) used. The data reported here are the average of the three readings from each experiment.

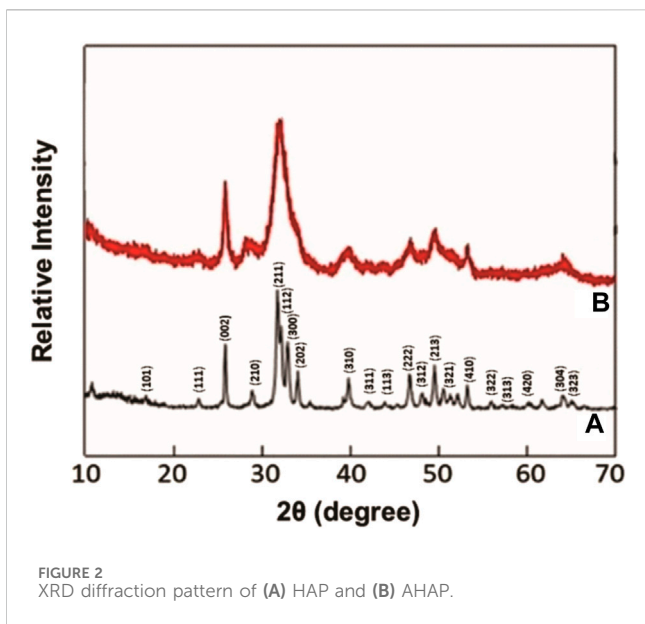
## 2.5 Artificial neural network (ANN) modeling

Applying an ANN model has recently been quite prevalent for predicting water quality. This study used a three-layered backpropagation neural network with a neural transfer function (purelin) at the output layer and a tangent sigmoid transfer function (tansig) at the hidden layer using MATLAB R2013a. The pH, contact time, and initial fluoride concentration were considered input parameters, and the percentage adsorption of fluoride was the output parameter. Of all the batch adsorption data sets, 70% was used for training, 15% for validation, and 15% for testing. All the data were normalized using the min-max normalization method to facilitate network learning and meet the required algorithm. This method normalizes the raw values in the range of 0–1 for better prediction and has the advantage of preserving all relationships in the data.

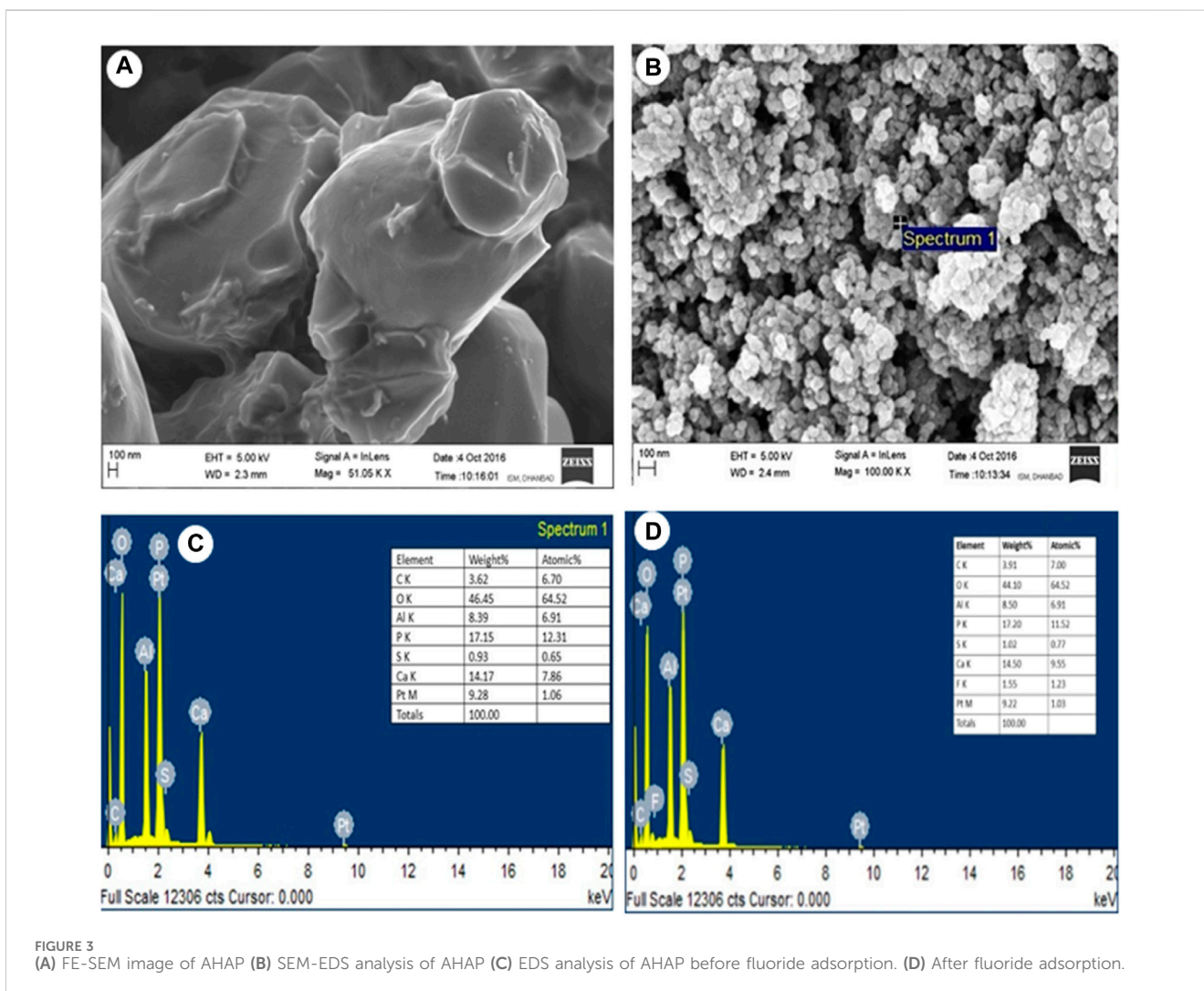
## 3 Results and discussions

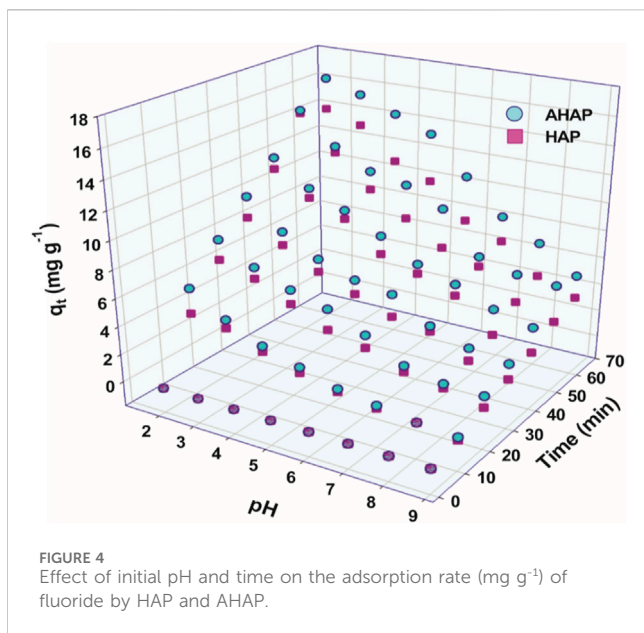
### 3.1 Characteristics of the nanosized HAP and AHAP

The surface area of the HAP and AHAP examined by the BET was  $154 \text{ m}^2 \text{ g}^{-1}$  and  $209 \text{ m}^2 \text{ g}^{-1}$ , respectively, indicating an enhancement in



surface area after alum doping. The smaller particle size of the metal ions-doped HAP increased surface area. Various studies have acknowledged the increase in surface area after doping HAP (Karunakaran et al., 2019). X-ray diffraction patterns of synthesized HAP and AHAP are represented in Figures 2A, B. XRD peaks were used to characterize the crystallographic evidence about the materials. The XRD spectra of the HAP spectra show its crystalline nature (Figure 2A), confirming the presence of crystalline HAP, as demonstrated by (101), (111), (002), (210), (211), (112), (300), (202), (310), (311), (113), (203), (222), (312), (213), (321), (410), (411), (322), (313), (304), and (323), respectively. In addition, the aluminum doping might induce phase transformations within the hydroxyapatite structure. This could result in the formation of new phases or the disruption of the original crystal lattice, leading to a reduction in crystallinity. The XRD patterns of the synthetic AHAP (Figure 2B) and those of HAP were nearly identical. No peaks that resemble alum were found. There is no significant change in the peak structure after the composition formation. This may be due to the incorporation of an aluminum compound into hydroxyapatite. Similar XRD patterns were reported by Nie et al. (2012) and Kolekar et al. (2016).





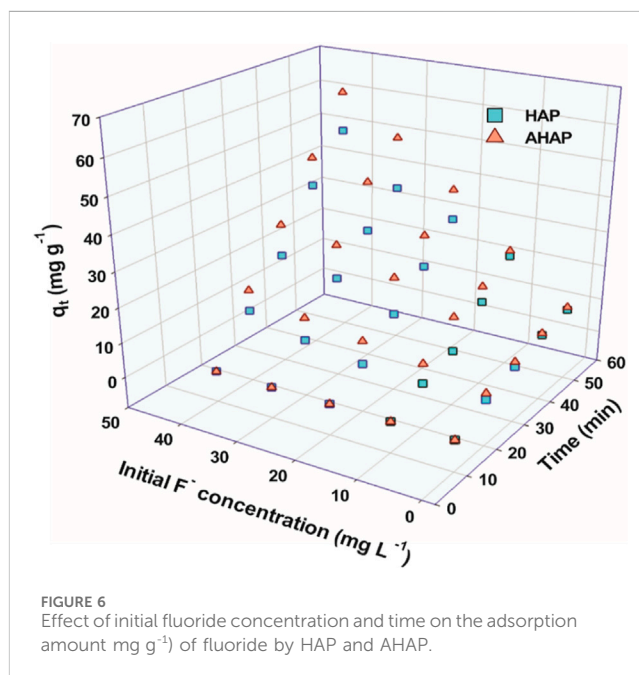
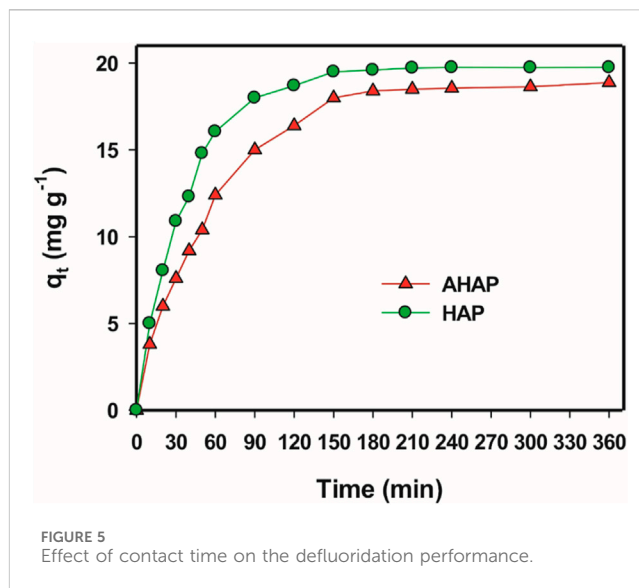
SEM-EDS spectra analysis was conducted to evaluate the morphology microstructure and for quantifiable elemental component analysis of HAP and AHAP samples. Figure 3A shows an FE-SEM image of HAP revealing two particles of different shapes attached, forming a highly porous structure. Figure 3B shows the signal-originated structure for Al and S in the EDS spectra due to alum doped on HAP. Figure 3C shows the EDS spectra after the adsorption of  $\text{F}^-$  onto HAP, and Figure 3D reveals surface adsorption of  $\text{F}^-$  onto AHAP.

### 3.2 Effect of pH

pH of the solution significantly affects the adsorption behaviors (Mahato and Gupta, 2020). It controls the adsorbent and adsorbate's surface charges in solution. The highest uptake of  $\text{F}^-$  was obtained at pH 2 for both HAP and AHAP, as shown in Figure 4. The adsorption of  $\text{F}^-$  decreased monotonously with an increase in the pH of the solution. This suggests that as pH values were increased, the presence of  $\text{OH}^-$  in the solution was increased, which could potentially compete with  $\text{F}^-$  for the adsorption sites. This could be due to the two ions with similar charge and ionic radius (Nie et al., 2012). AHAP was found to be insoluble in all pH studies, exhibiting its applicability at a wider pH range.

### 3.3 Effect of contact time

The outcomes of the study on the impact of interaction time on the adsorption of  $\text{F}^-$  by HAP and AHAP are shown in Figure 5. It can be observed from the figure that a quick removal of  $\text{F}^-$  takes place in the first 2 h, followed by a subsequent reduction in the rate of removal till equilibrium at 3 h. Additionally, it was found that as the contact time increased, so did the amount of adsorption. After 3 h, the maximum adsorption capacity for both HAP and AHAP



was achieved; afterward, there was almost no further increase in the adsorption. As a result, a fixed equilibrium contact time was chosen for the subsequent absorption experiment.

### 3.4 Effect of initial fluoride concentration

Figure 6 demonstrates the adsorption capacities of HAP and AHAP for  $\text{F}^-$ , through adsorbent-adsorbate solutions at different concentrations of fluoride (0.217–1.08 mM/L). Visibly the adsorbed amount of  $\text{F}^-$  increases by increasing the initial F-concentration. This is caused by the fact that there are more adsorbate ions present close to the adsorbents (Saber-Samandari et al., 2014).

### 3.5 Adsorption kinetics studies

The fluoride adsorption rate is highly dependent on contact time. To examine the dynamics of adsorption progression on HAP and AHAP, the pseudo-first-order, pseudo-second-order, Elovich, Bangham, and intraparticle diffusion models were applied. The pseudo-first-order rate reaction mechanism is explained in (Figure 7A). Pseudo-first-order equation is expressed as shown in Eq. (2):

$$\log(q_e - q_t) = \log q_e - \frac{t}{2.303}k_1 \tag{2}$$

where  $q_e$  and  $q_t$  ( $\text{mg g}^{-1}$ ) is the amount of  $\text{F}^-$  adsorbed at equilibrium and at time  $t$  (min), respectively, and  $k_1$  ( $\text{min}^{-1}$ ) is the pseudo-first-order rate constant. Mousa et al. (2016) proposed a kinetic experimental model based on the free sites between inter-particle diffusion. The pseudo-second-order model is used on the hypothesis that adsorption follows a

second-order mechanism, whereas the rate of sorption is proportional to the square of the number of untenanted sites (Ho et al., 2000). Pseudo-second-order equation is expressed as shown in Eq. 3.

$$\frac{t}{q_t} = \frac{1}{k_2 q_e^2} + \frac{t}{q_e} \tag{3}$$

where  $k_2$  represent the pseudo-second-order rate constant ( $\text{g mg}^{-1} \text{min}^{-1}$ ). The different parameters of the kinetics models are concisely shown in Table 1. The pseudo-second-order model can accurately represent the adsorption kinetics much more effectively than the pseudo-first-order model despite having strong correlation coefficients ( $R^2=0.9941$ ) Figure 7B and strong arrangements between experimental  $q_{\text{exp}}$  and calculated  $q_e$  values. In this instance, the adsorption of  $\text{F}^-$  is likely caused by surface complexation reactions at specific adsorption sites, and the adsorption rate-limiting step may be chemisorption (Ersan et al., 2015).

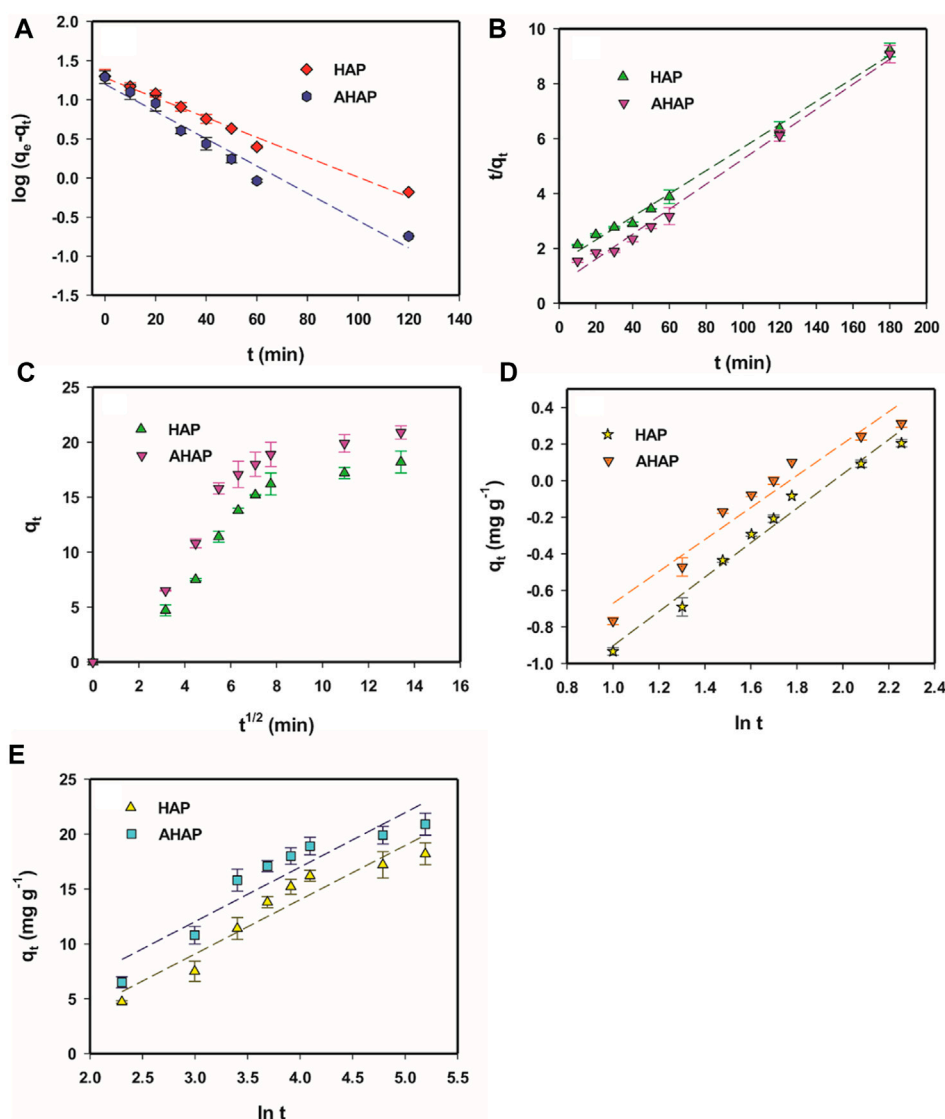


FIGURE 7 Pseudo first order plots for  $\text{F}^-$  adsorption (A), Pseudo second order plots (B), Intraparticle diffusion model plots (C), Bangham model plots (D), and Elovich plots (E).

TABLE 1 Kinetic parameters for F<sup>-</sup> adsorption using HAP and AHAP.

Kinetic models	Parameters	HAP	AHAP
Pseudo-first-order	$q_{e \text{ cal}}$ (mg/g)	18.10	15.990
	$k_1$ (min <sup>-1</sup> )	0.0292	0.0403
	R <sup>2</sup>	0.9862	0.9686
	$\chi^2$	0.231	0.211
pseudo-second-order	$q_{e \text{ cal}}$ (mg/g)	22.053	21.930
	$k_2$ (g/mg min)	0.001	0.003
	R <sup>2</sup>	0.9941	0.9918
	$\chi^2$	0.0038	0.0781
Intraparticle diffusion	$k_p$ (mg/g min)	1.443	1.580
	C	2.175	3.914
	R <sup>2</sup>	0.8531	0.8057
Elovich	$\alpha$ (mg/g min)	4.9022	22.318
	$\beta$ (g/mg)	0.297	0.339
	R <sup>2</sup>	0.8684	0.9024
	$\chi^2$	1.666	0.2119
Bangham	$\alpha$	0.941	0.873
	$k_B$ (g)	6.591	13.156
	R <sup>2</sup>	0.9780	0.9445
	$\chi^2$	0.1387	0.1925

This process is a rate preventive method and should be further envisaged. Pseudo-first-order and pseudo-second-order models cannot distinguish diffusion mechanisms during sorption. The diffusion mechanisms during the sorption process cannot be distinguished by pseudo-first-order or pseudo-second-order models. In order to better understand the intraparticle diffusion mechanism, Weber and Morris plots are useful as shown in Figure 7C, where  $q_t$  can be calculated using Eq. 4.

$$q_t = k_p t^{1/2} + C \quad (4)$$

Here,  $k_p$  and C represent intraparticle diffusion rate constant and intercept, respectively, in  $\text{mg g}^{-1} \text{min}^{-1/2}$ . When the diffusion mechanism is measured by intra-particle diffusion, the intercept C should cross the derivation (Saruchi, 2019). However, if the plot does not pass across the basis, as in this study, having an intercept (C) indicates the thickness of the boundary layer; a larger intercept suggests a greater boundary layer effect (Table 1). Additionally, it suggests that while intraparticle diffusion plays a role in adsorption, it is not the only rate-limiting mechanism. Other mechanisms, such as film diffusion, may also be involved. Most possibly, surface adsorption (pseudo-second-order) and intraparticle diffusion may occur simultaneously (Ghorai et al., 2013).

Adsorbate pore diffusion activities studied by the Bangham model (Figure 7D) which is expressed linearly as Eq. (5):

$$\log \log \left( \frac{C_0}{C_0 - q_t M} \right) = \log \left( \frac{M k_B}{2.303 V} \right) + \alpha \log t \quad (5)$$

where  $C_0$  is the initial concentration of F<sup>-</sup> ( $\text{mg L}^{-1}$ ), V is solution volume (mL), M is the adsorbent weight (g/L),  $q_t$  is the amount of adsorbate retained at time t ( $\text{mg g}^{-1}$ ), and  $\alpha$  ( $<1$ ),  $k_B$  are constants, which can be attained from slope and intercept, respectively. Bangham's plot should be linear if intraparticle diffusion is the only rate-controlling step. In the present study, the plot was in the linear form for each adsorbent with a good correlation coefficient value ( $>0.9$ ), suggesting that a pore diffusion mechanism governs the adsorption of fluoride onto HAP and AHAP.

Assuming that the actual solid surfaces are actively heterogeneous, the Elovich equation (Figure 7E) illustrates the second-order kinetic, but the equation does not suggest any specific mechanism for adsorbate-adsorbent interaction (Sparks, 1989). It is widely acknowledged that a semi-empirical equation can adequately describe the chemisorption process (Zhang and Stanforth, 2005) and can be expressed as Eq. (6).

$$q_t = \frac{1}{\beta} \ln(\alpha\beta) + \frac{1}{\beta} \ln(t) \quad (6)$$

where  $q_t$  ( $\text{mg g}^{-1}$ ) represents the amount of adsorbate adsorbed at time t,  $\alpha$  is a constant related to chemisorption rate, and  $\beta$  is a constant that illustrates the level of surface exposure. The two constants ( $\alpha$  and  $\beta$ ) were obtained from the intercept and slope of the plot of  $q_t$  versus  $\ln(t)$ , respectively, as shown in Table 1. The kinetic sorption curve fit well with the model with  $R^2 > 0.8684$  (Table 1). If the configuration is determined solely by equation, it may be assumed that diffusion is the rate-determining step, and this equation should apply in situations where the desorption rate can be neglected (Pavlatou and Polyzopouls, 1988; Rudzinski and Panczyk, 1998).

### 3.6 Adsorption isotherms

Adsorption isothermal studies of HAP and AHAP were carried out at different temperatures between 293 K and 313 K. Langmuir (1916), Freundlich (1906), and Temkin and Pyzhev, (1940) isotherm models have all been investigated to examine the synergistic behavior between the adsorbent and adsorbate molecules and the designed parameters are shown in Table 2. The Langmuir isotherm is valid for monolayer sorption because the surface is uniform and composed of a finite number of equivalent and identical localized sites, with no steric hindrance or lateral interaction between the adsorbed molecules, even on adjacent sites. According to the Langmuir Isotherm, the sorption of pollutants on solids can be described by Eq. 7:

$$\frac{1}{q_e} = \frac{1}{Q} + \frac{1}{Q K_L} \cdot \frac{1}{C_e} \quad (7)$$

where,  $q_e$  = fluoride removal capacity at equilibrium ( $\text{mg g}^{-1}$ ); Q = maximum monolayer coverage capacities ( $\text{mg g}^{-1}$ );  $K_L$  = Langmuir isotherm constant ( $\text{L mg}^{-1}$ );  $C_e$  = at equilibrium concentration ( $\text{mg L}^{-1}$ ). Plot of  $1/q_e$  vs.  $1/C_e$  yields the values of slope and intercept from which the values of  $K_L$  and Q were

TABLE 2 Parameters for different isotherm models for F<sup>-</sup> adsorption using AHAP.

Models	Parameters	HAP			AHAP		
		Temperature (K)			Temperature (K)		
		293 K	293 K	303 K	293 K	293 K	303 K
Langmuir	$Q$ (mg g <sup>-1</sup> )	40.59	45.66	48.05	53.19	58.14	68.19
	$b$ (L mg <sup>-1</sup> )	0.520	0.595	0.627	0.598	0.612	0.653
	$R_L$	0.0188	0.0165	0.0157	0.0160	0.0161	0.0151
	$R^2$	0.9425	0.9489	0.9408	0.9894	0.9931	0.9872
	$\chi^2$	0.0052	0.0065	0.0048	0.0047	0.0066	0.0002
Freundlich	$K_f$ (mg g <sup>-1</sup> )	13.00	14.19	14.98	4.402	5.922	7.532
	$n$	3.05	2.61	2.37	1.153	1.073	0.952
	$R^2$	0.8690	0.9113	0.9296	0.9279	0.9363	0.9279
	$\chi^2$	0.0082	0.080	0.052	0.0482	0.0081	0.0004
Temkin	$K_t$ (L g <sup>-1</sup> )	3.923	3.365	3.271	4.300	5.438	6.539
	$B$	9.9115	10.725	13.073	12.154	12.465	14.150
	$\beta$ (J mol <sup>-1</sup> )	245.75	234.88	199.06	200.42	202.09	183.91
	$R^2$	0.9118	0.9257	0.9026	0.9369	0.9158	0.8683
	$\chi^2$	2.880	6.751	8.226	6.472	7.008	7.242

calculated. The computed maximum adsorption capability ( $Q$ ) for AHAP was 0.905 mL<sup>-1</sup> at 40°C, suggesting significantly larger adsorption than HAP (0.558 mL<sup>-1</sup>). According to Ayad and El-Nasar (2010), an important characteristic of the Langmuir isotherm can be expressed in terms of a dimensionless factor called the separation factor ( $R_L$ ), which is defined by the following Eq. (8):

$$R_L = \frac{1}{1 + K_L C_0} \quad (8)$$

where  $K_L$  (L mg<sup>-1</sup>) is the Langmuir constant relates to the heat of adsorption and  $C_0$  is the initial concentration of F<sup>-</sup> (mg L<sup>-1</sup>). The isotherm's shape is determined by the value of  $R_L$ , which can be unfavorable ( $R_L > 1$ ), linear ( $R_L = 1$ ), irreversible ( $R_L = 0$ ), or favorable ( $0 < R_L < 1$ ).  $R_L$  was between zero and unity, indicating that F<sup>-</sup> adsorption was advantageous, and as the temperature rose, it got closer to zero, indicating irreversible adsorption (Ghorai et al., 2013).

The Freundlich isotherm assumes that multilayer sorption occurs to take up F<sup>-</sup> molecules on a heterogeneous surface. Eq. 9 is given below and represents the linear form of the Freundlich isotherm model.

$$\log q_e = \log K_f + \frac{1}{n} \cdot \log C_e \quad (9)$$

Where  $C_e$  = equilibrium concentration (mg L<sup>-1</sup>);  $n$  = adsorption intensity;  $q_e$  = amount of adsorbate in the adsorbent at equilibrium (mg g<sup>-1</sup>);  $K_f$  = Freundlich isotherm constant (mg g<sup>-1</sup>) proportional to adsorption capacity. The applicability of the Freundlich equation was indicated by the linear plot of  $\log q_e$  vs  $\log C_e$ . The value of  $1/n$  determined from the Freundlich isotherm plot denotes adsorption intensity. Generally,  $0.1 < 1/n < 0.5$  is regarded as easily absorbing;

$0.5 < 1/n < 1$ , some difficulties exist with the adsorption;  $1/n > 1$ , it is quite difficult to adsorb (Ozbay et al., 2013). When the F<sup>-</sup> ions were either simple to adsorb or there were some challenges, the scale of variation in  $1/n$ , with a value ranging from 0.5 to 0.56, became apparent, accelerating with an increase in reaction temperature. Moreover, a value of  $1/n$  below unity in this study implies the occurrence of the chemisorption process (Wu, 2007).

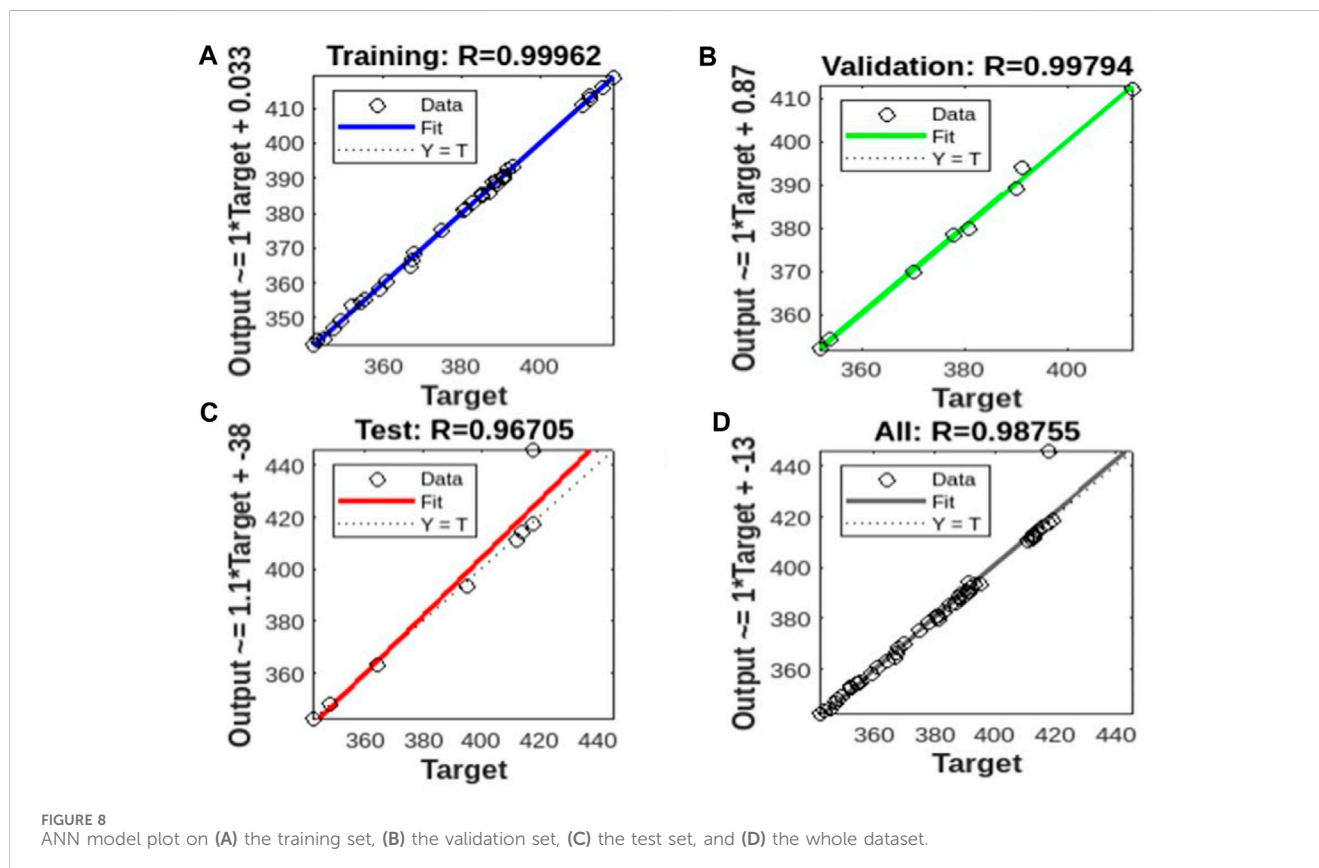
Temkin isotherm model, specifically takes adsorbing species-adsorbent interactions into account. Adsorbent-adsorbate interactions cause all of the molecules in the layer's heat of adsorption to fall linearly with surface coverage. The adsorption is assumed to be characterized by a continuous distribution of binding energies up to a maximum binding energy (Temkin and Pyzhev, 1940; Mall et al., 2005). The linear form of Temkin isotherm equation is given as shown in Eq. 10.

$$q_e = B \ln K_T + B \ln C_e \quad (10)$$

where  $B = \frac{RT}{\beta}$ , and  $K_T$  is the Temkin isotherm constant (L g<sup>-1</sup>),  $\beta$  is the Temkin constant related to the heat of sorption (J mol<sup>-1</sup>),  $R$  is the gas constant (8.314 J mol<sup>-1</sup> K<sup>-1</sup>), and  $T$  is the absolute temperature (K). Temkin isotherm parameters were obtained by plotting the quantity sorbed  $q_e$  against  $\ln C_e$ . Linear plots for the Temkin adsorption isotherm, which account for the chemisorption of an adsorbent on the adsorbent, fit very well with the correlation coefficients  $\geq 0.93$  (Table 3). This further supports the findings that the adsorption of F<sup>-</sup> onto HAP and AHAP is a chemisorption process. The value of the Langmuir constant ( $K_L$ ), Freundlich constant ( $K_f$ ), and Temkin isotherm constant ( $K_T$ ) increased with temperature, indicating a greater affinity at higher temperatures between the active sites of the adsorbent and the

TABLE 3 Thermodynamic parameters for the adsorption of F<sup>-</sup> using AHAP.

Adsorbent	-ΔG (kJ mol <sup>-1</sup> )			ΔS (kJ mol <sup>-1</sup> K <sup>-1</sup> )	ΔH (kJ mol <sup>-1</sup> )
	293 K	303 K	313 K		
AHAP	-0.306	-0.406	-0.412	1.95	0.005
HAP	-0.425	-0.763	-1.577	7.509	0.023



adsorbate. Also, it reveals the endothermic nature of the adsorption process. Based on chi-square test statistics and regression coefficients, these steps led to the best-fit model: For fluoride sorption onto HAP and AHAP, Langmuir > Freundlich > Temkin. Therefore, the Langmuir model ( $R^2=0.9425$ ) is the best-fit isotherm equation for the adsorption of F<sup>-</sup> onto HAP and AHAP.

### 3.7 Thermodynamic study

Thermodynamic parameters, like change in Gibb's free energy ( $\Delta G^\circ$ ), and can be calculated using Eqs (11)–(12), change in entropy ( $\Delta S^\circ$ ), and change in enthalpy ( $\Delta H^\circ$ ) were calculated using Van't Hoff's equation from a plot of  $\ln K_L$  versus  $1/T$  and are documented in Table 3.

$$\Delta G^\circ = -RT \ln K_L \quad (11)$$

$$\ln K_L = -\frac{\Delta G^\circ}{RT} = \frac{\Delta S^\circ}{R} - \frac{\Delta H^\circ}{RT} \quad (12)$$

where,  $K_L$  = Langmuir adsorption constant (L mg<sup>-1</sup>);  $\Delta S^\circ$  = adsorption entropy (J mol<sup>-1</sup> K<sup>-1</sup>);  $\Delta H^\circ$  = apparent enthalpy of adsorption (kJ mol<sup>-1</sup>);  $\Delta G^\circ$  = adsorption free energy (kJ mol<sup>-1</sup>);  $R$  = gas constant (0.008314 kJ mol K<sup>-1</sup>);  $T$  = solution temperature (K). The experimental values of  $\Delta G^\circ$ ,  $\Delta S^\circ$  and  $\Delta H^\circ$  were determined from the linear plot of  $\ln K_L$  vs.  $1/T$ . The endothermic nature of adsorption is confirmed by the positive values of  $\Delta H^\circ$  and  $\Delta S^\circ$ , which is supported by the increase in the adsorption of F<sup>-</sup> with temperature. It might be due to the displaced water molecules' higher translational entropy acquisition than the entropy lost due to F<sup>-</sup> uptake onto HAP and AHAP. It is evident that all of the tested temperatures had negative free energy values ( $\Delta G^\circ$ ). The positive  $\Delta S^\circ$  value implied that the adsorption reaction is related to a dissociative mechanism and improved randomness during adsorption because  $\Delta S^\circ > -10^{-2}$  kJ mol<sup>-1</sup> typically denotes a dissociative mechanism (Aksu and Isoglu, 2005). The higher translational entropy might cause the displaced water molecules to be acquired compared to what was lost from F<sup>-</sup> uptake onto HAP and AHAP. All the tested temperatures had negative free energy values ( $\Delta G^\circ$ ). This demonstrates that the adsorption is

spontaneous and advantageous from a thermodynamic standpoint. Additionally, the greater driving force of adsorption implied by the more negative value of ( $\Delta G^\circ$ ) with a temperature rise indicated a higher adsorption capacity (Saber-Samandari et al., 2014).

### 3.8 ANN simulation of AHAP's adsorption efficiency

The ANN model obtained a good relationship from the training data and performed relatively well in the validation and testing (Figures 8A–D). The value of correlation coefficients ( $R^2$ - 0.9996) also confirms the predictive ability of the ANN model for the simulation of the adsorption efficiency of AHAP. Overall, the ANN modeling approach performed satisfactorily for the batch adsorption experimental dataset of the present study. The higher generalization capacity of ANN increased its tolerance to noisy data, eliminating the chances of any biased prediction (Mahato and Gupta, 2022).

## 4 Conclusion

HAP and AHAP were synthesized biomimetically using a chemical co-precipitation technique.

Both adsorbents exhibited the effective capability of defluoridation under acidic conditions. However, the maximum fluoride adsorption capacity of AHAP (68.19 mg/g) was observed to be higher than HAP (48.05 mg/g), which was attributed to the alum doping. The Langmuir isotherms model was more suitable for fitting experimental data, demonstrating the monolayer adsorption process. The application of ANN modeling best simulated ( $R^2$ - 0.9996) the adsorptive efficiency of AHAP. The study provides promising development direction of AHAP for effective and environmentally safe defluoridation.

## Data availability statement

The raw data supporting the conclusion of this article will be made available by the authors, without undue reservation.

## References

- Ahmad, M. A., Ahmad, N., and Bello, O. S. (2015). Modified durian seed as adsorbent for the removal of methyl red dye from aqueous solutions. *Appl. Water Sci.* 5, 407–423. doi:10.1007/s13201-014-0208-4
- Aksu, Z., and Isoglu, I. A. (2005). Removal of copper (II) ions from aqueous solution by biosorption onto agricultural waste sugar beet pulp. *Process Biochem.* 40, 3031–3044. doi:10.1016/j.procbio.2005.02.004
- Ali, S., Mahato, K., Gupta, S. K., Sinha, A., and Islam, R. (2021). Defluoridation of ground-water using formaldehyde-treated agricultural waste-wheat, oats, and pea straw. *Earth Environ. Sci. Res.* 4 (2), 109–115.
- Amalraj, A., and Pius, A. (2017). Removal of fluoride from drinking water using aluminium hydroxide coated activated carbon prepared from bark of *Moringa tinctoria*. *Appl. Water Sci.* 7, 2653–2665. doi:10.1007/s13201-016-0479-z
- Ayad, M. M., and El-Nasr, A. A. (2010). Adsorption of cationic dye (methylene blue) from water using polyaniline nanotubes base. *J. Phys. Chem. C* 114, 14377–14383. doi:10.1021/jp103780w
- Ayoub, S., and Gupta, A. K. (2006). Fluoride in drinking water: a review on the status and stress effects. *Crit. Rev. Environ. Sci. Technol.* 36 (6), 433–487. doi:10.1080/10643380600678112
- Bhatnagar, A., Kumar, E., and Sillanpää, M. (2011). Fluoride removal from water by adsorption- A review. *Chem. Eng. J.* 171 (3), 811–840. doi:10.1016/j.cej.2011.05.028
- Chen, N., Zhang, Z., Feng, C., Zhu, D., Yang, Y., and Sugiura, N. (2011). Preparation and characterization of porous granular ceramic containing dispersed aluminum and iron oxides as adsorbents for fluoride removal from aqueous solution. *J. Hazard. Mater.* 186, 863–868. doi:10.1016/j.jhazmat.2010.11.083
- Choubisa, S. L., Choubisa, D., and Choubisa, A. (2023). Fluoride contamination of groundwater and its threat to health of villagers and their domestic animals and agriculture crops in rural Rajasthan, India. *Environ. Geochem. Health* 45 (3), 607–628. doi:10.1007/s10653-022-01267-z
- Chouhan, S., and Flora, S. J. S. (2010). Arsenic and fluoride: two major ground water pollutants. *Indian J. Exp. Biol.* 48, 666–678.
- Ersan, M., Guler, U. A., Acikel, U., and Sarioglu, M. (2015). Synthesis of hydroxyapatite/clay and hydroxyapatite/pumice composites for tetracycline removal from aqueous solutions. *Process Saf. Environ. Prot.* 96, 22–32. doi:10.1016/j.psep.2015.04.001
- Freundlich, H. M. F. (1906). Über die Adsorption in Lösungen. *Z. für Phys. Chem.* 57, 385–470. doi:10.1515/zpch-1907-5723
- Ghorai, S., Sarkar, A. K., Panda, A. B., and Pal, S. (2013). Effective removal of Congo red dye from aqueous solution using modified xanthan gum/silica hybrid nanocomposite as adsorbent. *Bioresour. Technol.* 144, 485–491. doi:10.1016/j.biortech.2013.06.108

## Author contributions

NV: Writing–original draft. AS: Supervision, Writing–original draft, Writing–review and editing. SG: Conceptualization, Writing–review and editing. JM: Conceptualization, Investigation, Writing–review and editing. PC: Data curation, Writing–review and editing.

## Funding

The author(s) declare that no financial support was received for the research, authorship, and/or publication of this article.

## Acknowledgments

The authors thank the Department of Environmental Science and Engineering, Indian Institute of Technology (Formality Indian School of Mines), Dhanbad-826004, India, for providing the necessary facilities for conducting these experiments.

## Conflict of interest

The authors declare that the research was conducted in the absence of any commercial or financial relationships that could be construed as a potential conflict of interest.

## Publisher's note

All claims expressed in this article are solely those of the authors and do not necessarily represent those of their affiliated organizations, or those of the publisher, the editors and the reviewers. Any product that may be evaluated in this article, or claim that may be made by its manufacturer, is not guaranteed or endorsed by the publisher.

- Ho, Y. S., McKay, G., Wase, D. J., and Foster, C. F. (2000). Study of the sorption of divalent metal ions on peat. *Adsorpt. Sci. Technol.* 18, 639–650. doi:10.1260/0263617001493693
- Jagtap, S., Yenkie, M. K., Labhsetwar, N., and Rayalu, S. (2012). Fluoride in drinking water and defluoridation of water. *Chem. Rev.* 112 (4), 2454–2466. doi:10.1021/cr2002855
- Karunakaran, G., Cho, E.-B., Kumar, G. S., Kolesnikov, E., Janarthanan, G., Pillai, M. M., et al. (2019). Ascorbic acid-assisted microwave synthesis of mesoporous Ag-doped hydroxyapatite nanorods from biowaste seashells for implant applications. *ACS Appl. Bio Mater.* 2, 2280–2293. doi:10.1021/acsabm.9b00239
- Kolekar, T. V., Thorat, N. D., Yadav, H. M., Magalad, V. T., Shinde, M. A., Bandgar, S. S., et al. (2016). Nanocrystalline hydroxyapatite doped with aluminium: a potential carrier for biomedical applications. *Ceram. Int.* 42, 5304–5311. doi:10.1016/j.ceramint.2015.12.060
- Lacson, C. F. Z., Lu, M.-C., and Huang, Y.-H. (2021). Fluoride-containing water: a global perspective and a pursuit to sustainable water defluoridation management -An overview. *J. Clean. Prod.* 280, 124236. doi:10.1016/j.jclepro.2020.124236
- Langmuir, I. (1916). The constitution and fundamental properties of solids and liquids. *J. Am. Chem. Soc.* 38, 2221–2295. doi:10.1021/ja02268a002
- Loganathan, P., Vigneswaran, S., Kandasamy, J., and Naidu, R. (2013). Defluoridation of drinking water using adsorption processes. *J. Hazard. Mater.* 248 (249), 1–19. doi:10.1016/j.jhazmat.2012.12.043
- Mahato, J. K., and Gupta, S. K. (2020). Modification of Bael fruit shell and its application towards Natural organic matter removal with special reference to predictive modeling and control of THMs in drinking water supplies. *Environ. Technol. Innovation* 18, 100666. doi:10.1016/j.eti.2020.100666
- Mahato, J. K., and Gupta, S. K. (2022). Exploring applicability of artificial intelligence and multivariate linear regression model for prediction of trihalomethanes in drinking water. *Int. J. Environ. Sci. Technol.* 19 (6), 5275–5288. doi:10.1007/s13762-021-03392-1
- Mall, I. D., Srivastava, V. C., Agarwal, N. K., and Mishra, I. M. (2005). Removal of conged from aqueous solution by bagasse fly ash and activated carbon: kinetic study and equilibrium isotherm analyses. *Chemosphere* 61, 492–501. doi:10.1016/j.chemosphere.2005.03.065
- Mohapatra, M., Anand, S., Mishra, B. K., Giles, D. E., and Singh, P. (2009). Review of fluoride removal from drinking water. *J. Environ. Manag.* 91 (1), 67–77. doi:10.1016/j.jenvman.2009.08.015
- Mousa, S. M., Ammar, S. N., and Ibrahim, H. A. (2016). Removal of lead ions using hydroxyapatite nano-material prepared from phosphogypsum waste. *J. Saudi Chem. Soc.* 20, 357–365. doi:10.1016/j.jscs.2014.12.006
- Nie, Y., Hu, C., and Kong, C. (2012). Enhanced fluoride adsorption using Al (III) modified calcium hydroxyapatite. *J. Hazard. Mater.* 233–234, 194–199. doi:10.1016/j.jhazmat.2012.07.020
- Nkansah, M. A., Dua, A. B., Aryee, G. A., and Adusei-Gyamfi, J. (2022). Evaluation of scales of Tilapia sp. and sciaenops ocellatus as low cost and green adsorbent for fluoride removal from water. *Front. Chem.* 10, 813533. doi:10.3389/fchem.2022.813533
- Ozbay, İ., Ozdemir, U., Ozbay, B., and Veli, S. (2013). Kinetic, thermodynamic, and equilibrium studies for adsorption of azo reactive dye onto a novel waste adsorbent: charcoal ash. *Desalination Water Treat.* 51 (31–33), 6091–6100. doi:10.1080/19443994.2013.763387
- Pavlatou, A., and Polyzopoulis, N. A. (1988). The role of diffusion in the kinetics of phosphate desorption: the relevance of the Elovich equation. *Eur. J. Soil Sci.* 39, 425–436. doi:10.1111/j.1365-2389.1988.tb01228.x
- Prasad, K. S., Amin, Y., and Selvaraj, K. (2014). Defluoridation using biomimetically synthesized nano zirconium chitosan composite: kinetic and equilibrium studies. *J. Hazard. Mater.* 276, 232–240. doi:10.1016/j.jhazmat.2014.05.038
- Rudzinski, W., and Panczyk, P. (1998). in *Surfaces of nanoparticles and porous materials*. Editors J. A. Schwarz and C. I. Contescu (New York: Dekker), 355.
- Saber-Samandari, S., Saber-Samandari, S., Nezafati, N., and Yahya, K. (2014). Efficient removal of lead (II) ions and methylene blue from aqueous solution using chitosan/Fe-hydroxyapatite nanocomposite beads. *J. Environ. Manag.* 146, 481–490. doi:10.1016/j.jenvman.2014.08.010
- Saruchi, K. V. (2019). Adsorption kinetics and isotherms for the removal of rhodamine B dye and Pb<sup>2+</sup> ions from aqueous solutions by a hybrid ion-exchanger. *Arabian J. Chem.* 12 (3), 316–329. doi:10.1016/j.arabj.2016.11.009
- Sasaki, K., Nagato, S., Ideta, K., Miyawaki, J., and Hirajima, T. (2017). Enhancement of fluoride immobilization in apatite by Al<sup>3+</sup> additives. *Chem. Eng. J.* 311, 284–292. doi:10.1016/j.ccej.2016.11.096
- Shaji, E., Sarath, K. V., Santosh, M., Krishnaprasad, P. K., Arya, B. K., and Babu, M. S. (2024). Fluoride contamination in groundwater: a global review of the status, processes, challenges, and remedial measures. *Geosci. Front.* 15 (2), 101734. doi:10.1016/j.gsf.2023.101734
- Singh, J., Singh, P., and Singh, A. (2016). Fluoride ions vs removal technologies: a study. *Arabian J. Chem.* 9, 815–824. doi:10.1016/j.arabj.2014.06.005
- Singh, Y., Solanki, M. A., Gupta, A. B., SanjeevGupta, P. S., and Shukla, P. (2022). Fluoride occurrences, health problems, detection, and remediation methods for drinking water: a comprehensive review. *Sci. Total Environ.* 807, 150601. doi:10.1016/j.scitotenv.2021.150601
- Sinha, A., Nayar, S., Agrawal, A., Bhattacharyya, D., and Ramachandrarao, P. (2003). Synthesis of nanosized and microporous precipitated hydroxyapatite in synthetic polymers and biopolymers. *J. Am. Ceram. Soc.* 86, 357–359. doi:10.1111/j.1151-2916.2003.tb00024.x
- SinhaMishra, A. T., and Ravishankar, N. (2008). Polymer assisted hydroxyapatite microspheres suitable for biomedical application. *J. Mater. Sci. Mater. Med.* 19, 2009–2013. doi:10.1007/s10856-007-3286-0
- Sparks, D. L. (1989). *Kinetics of soil chemical processes*. San Diego, California: Academic Press.
- Tang, J., Xiang, B., Li, Y., Tan, T., and Zhu, Y. (2022). Adsorption characteristics and charge transfer kinetics of fluoride in water by different adsorbents. *Front. Chem.* 10, 917511. doi:10.3389/fchem.2022.917511
- Temkin, M. J., and Pyzhev, V. (1940). Recent modifications to Langmuir isotherms. *Acta Physicochem. URSS* 12, 217–222.
- Tripathy, S. S., Bersillon, J. L., and Gopal, K. (2006). Removal of fluoride from drinking water by adsorption onto alum-impregnated activated alumina. *Sep. Purif. Technol.* 50, 310–317. doi:10.1016/j.seppur.2005.11.036
- Who, (2008). *Guidelines for drinking water quality incorporating 1<sup>st</sup> and 2<sup>nd</sup> addenda, recommendations*. 3rd edn. Geneva: World Health Organization.
- Wu, C. H. (2007). Adsorption of reactive dye onto carbon nanotubes: equilibrium, kinetics and thermodynamics. *J. Hazard. Mater.* 144, 93–100. doi:10.1016/j.jhazmat.2006.09.083
- Xiong, X., Liu, J., He, W., Xia, T., He, P., Chen, X., et al. (2007). Dose-effect relationship between drinking water fluoride levels and damage to liver and kidney functions in children. *Environ. Res.* 103, 112–116. doi:10.1016/j.envres.2006.05.008
- Yang, K., Liang, X., and Quan, C. (2019). *Reference module in earth systems and environmental sciences*. Amsterdam, Netherlands: Elsevier, 34. doi:10.1016/B978-0-12-409548-9.11083-8
- Zhang, J., and Stanforth, R. (2005). Slow adsorption reaction between arsenic species and goethite ( $\alpha$ -FeOOH): diffusion or heterogeneous surface reaction control. *Langmuir* 21 (7), 2895–2901. doi:10.1021/la047636e